NACA

RESEARCH MEMORANDUM

INVESTIGATION OF TURBINES SUITABLE FOR USE IN A TURBOJET

ENGINE WITH HIGH COMPRESSOR PRESSURE RATIO

AND LOW COMPRESSOR-TIP SPEED

V - EXPERIMENTAL PERFORMANCE OF TWO-STAGE TURBINE

WITH DOWNSTREAM STATOR

By Elmer H. Davison, Donald A. Petrash, and Harold J. Schum

Lewis Flight Propulsion Laboratory Cleveland, Ohio

NATIONAL ADVISORY COMMITTEE FOR AERONAUTICS

WASHINGTON

October 21, 1955 Declassified October 28, 1960

NATIONAL ADVISORY COMMITTEE FOR AERONAUTICS

RESEARCH MEMORANDUM

INVESTIGATION OF TURBINES SUITABLE FOR USE IN A TURBOJET ENGINE WITH

HIGH COMPRESSOR PRESSURE RATIO AND LOW COMPRESSOR-TIP SPEED

V - EXPERIMENTAL PERFORMANCE OF TWO-STAGE TURBINE

WITH DOWNSTREAM STATOR

By Elmer H. Davison, Donald A. Petrash, and Harold J. Schum

SUMMARY

As part of a general study of obtaining high work output at low blade speeds with multistage turbines, a two-stage turbine with a down-stream stator was experimentally investigated. High Mach numbers, high turning angles, low static-pressure drops across blade rows, and large tangential components of velocity at the exit of the second rotor made this a critical turbine design. A downstream stator was employed to recover the energy of the tangential velocity at the exit of the second rotor.

The turbine passed 0.98 of the equivalent design weight flow at equivalent design speed and work. The brake internal efficiency at this point was 0.81 and occurred at a rating pressure ratio of 3.8. A maximum efficiency of 0.85 occurred at 130 percent of equivalent design speed and a work output of 36.5 Btu per pound, corresponding to a rating pressure ratio of approximately 4.4.

The downstream stator left very little energy in the form of tangential velocity in the gas at any operating condition. At equivalent design work and speed, the downstream stator recovered 0.78 of the energy of the tangential velocity entering the stator. The energy of this tangential velocity amounted to 4.8 points in turbine efficiency.

INTRODUCTION

The NACA Lewis laboratory is currently conducting a general study of high-work-output, low-speed, multistage turbines. As part of this study, the design requirements of turbines to drive a particular single-spool, high-pressure ratio, low-blade-tip-speed compressor at several

engine operating conditions were investigated (ref. 1). Studies were made to determine the turbine velocity diagrams for the turbine requirements imposed by engine operation with constant exhaust-nozzle area (ref. 2) and engine operation at constant design rotative speed (ref. 3). The turbine design requirements for engine operation at constant design rotative speed were more critical than those for engine operation with constant exhaust-nozzle area, and it was necessary to incorporate a downstream stator behind a two-stage turbine in order to obtain reasonable velocity diagrams. These velocity diagrams had higher Mach numbers, greater turning within blade rows, and lower static-pressure drops across some of the blade rows than those used in conventional turbine designs. Less critical turbine aerodynamic designs could, of course, have been obtained with a three-stage turbine or by increasing the design rotative speed, as discussed in reference 4.

Although the two-stage turbine design for engine operation with constant exhaust-nozzle area and the two-stage turbine design with a downstream stator for engine operation at constant design rotative speed were critical, reasonably good turbine performance appeared to be feasible. In order to obtain the performance of such a turbine design, the two-stage turbine with a downstream stator was fabricated and investigated as a component with cold-air turbine-inlet conditions. The purpose of this report, then, is to (1) present the over-all performance of this turbine and (2) evaluate the downstream stator in terms of turbine over-all performance.

The turbine was operated at a constant inlet total (stagnation) pressure of 35 inches of mercury absolute and an inlet total temperature of 700° R. Over-all turbine performance characteristics were obtained over a range of pressure ratios and speeds. These performance results are presented in terms of brake internal efficiency, equivalent work output, equivalent weight flow, and equivalent rotor speed. The effectiveness of the downstream stator in recovering the energy of the second rotor-exit tangential velocity over a range of turbine operating conditions is presented. A brief description of the method used to design the blade profiles is included. Also presented herein are the choking characteristics of the turbine obtained from the interstage static-pressure measurements.

SYMBOLS

The following symbols are used in this report:

- A annular area, sq ft
- specific heat at constant pressure, Btu/(lb)(OR)
- E enthalpy drop (based on measured torque), Btu/lb

CG-1 back

g gravitational constant, 32.174 ft/sec²

J mechanical equivalent of heat, 778 ft-lb/Btu

N rotational speed, rpm

p static pressure, lb/sq ft

p' total pressure, lb/sq ft

p' rating total pressure, static pressure plus velocity pressure corresponding to axial component of velocity, lb/sq ft

R gas constant, 53.4 ft-lb/(lb)(OR)

S entropy

T static temperature, OR

T' total temperature, OR

static temperature plus velocity temperature corresponding to axial component of velocity, OR

velocity, ft/sec

w weight flow, lb/sec

 $\frac{\text{wN}}{60\delta}$ ϵ weight-flow parameter based on equivalent weight flow and equivalent rotor speed

γ ratio of specific heats

ratio of inlet-air pressure to NACA standard sea-level pressure, p'/2116

function of
$$\gamma$$
, $\frac{\gamma_{sl}}{\gamma_{e}} = \frac{\left(\frac{\gamma_{e}+1}{2}\right)^{\gamma_{e}-1}}{\frac{\gamma_{sl}}{\gamma_{sl}-1}}$

- η brake internal efficiency, ratio of actual turbine work based on torque measurements to ideal turbine work
- $\theta_{\rm cr}$ squared ratio of critical velocity to critical velocity at NACA standard sea-level temperature of 518.7° R, $\frac{2\gamma}{\gamma+1} \, {\rm gRT}_0^{\prime}$ $\frac{2\gamma_{\rm sl}}{\gamma_{\rm sl}+1} \, {\rm gRT}_{\rm sl}^{\prime}$
- ρ static density, lb/cu ft
- τ torque, ft-lb

Subscripts:

- e engine operating conditions
- sl NACA standard sea-level conditions
- u tangential
- x axial
- 0,1, 2,3, measuring stations (see fig. 2)

APPARATUS

Test Installation

The experimental setup of the turbine is shown in figure 1. The air weight flow through the turbine was measured by a submerged calibrated A.S.M.E. flange-tap flat-plate orifice. After metering, the air was throttled to the desired turbine-inlet pressure of 35 inches of mercury absolute. A portion of this air was heated by two commercial jet-engine burners and reintroduced into the main air stream. The resulting turbine-inlet temperature after mixing was maintained at 700° R. The air weight flow through the turbine was corrected for the fuel addition by measuring the fuel flow with rotameters in the fuel line. The air flow divided and entered a plenum chamber (which replaced the normal combustion-can assembly of an engine) through two openings 180° apart and at right angles to the turbine shaft. The air then passed through a screen and into 10 transition sections, each of which supplied air to a segment of the first-stage stator. The air passed through the turbine into the tail cone, whence it was discharged into the laboratory exhaust facilities.

Two 5000-horsepower cradled dynamometers of the eddy-current wetgap type were connected in tandem and were used to absorb the power output of the turbine. The turbine torque output was measured by means of an NACA balanced-diaphragm thrust meter. The turbine rotative speed was measured by means of an electric chronometric tachometer.

Instrumentation

The instrumentation used for the performance evaluation of the turbine and downstream stator was located at stations 0, 5, and 6, as shown in figure 2. The turbine-inlet conditions at station 0 were measured by means of a combination probe consisting of a shielded totalpressure tube and a calibrated spike-type thermocouple, and two wall static-pressure taps in each of the 10 transition sections. The instrumentation installed in station 5 consisted of five shielded totalpressure probes located at different radii corresponding to the area centers of five equal-annular areas and of four wall static-pressure taps on both the inner and outer shroud. Total-pressure probes and wall static taps (increased to eight on both the inner and outer shroud) were installed in a similar manner at station 6. Four thermocouple rakes were also installed at station 6. Each thermocouple rake consisted of five spike-type thermocouples located such that duplicate temperatures at 10 radial positions at the area centers of equal-annular areas were obtained with the four rakes. Photographs of the instruments used are shown in figure 3. At stations 2 to 4, four wall staticpressure taps on both the inner and outer shroud were installed (see fig. 2). Two wall static-pressure taps were also installed in each transition section at station 1. At stations 1 to 5 the wall static-pressure taps were located midway circumferentially between adjacent stator blades. The total-pressure probes at station 5 were installed in like manner.

TURBINE AND BLADE DESIGN

Velocity Diagrams

The design velocity diagrams and the method used to select them are presented in reference 3. In calculating the design velocity diagrams at stations 2 to 5, a free-vortex distribution of tangential velocity and simple radial equilibrium were assumed. Radial components of velocity were ignored in calculating the velocity diagrams as well as in the design of the blade profiles. These design velocity diagrams are reproduced from reference 3 and presented in figure 4.

Turbine Blade Profile Design

With exception of the downstream stator, the blade profiles were designed using a two-dimensional quasi-channel-flow theory and a stream-filament technique developed in reference 5.

Three flow regions were examined for each constant-radius blade passage design. These three regions consisted of (1) the section between the passage potential line where the flow first becomes fully contained within the blade passage and the passage potential line at the throat of the blades, (2) the portion of the blade downstream of the throat, and (3) the leading-edge section of the blade. The design procedure consisted of mating these three flow regions by means of judicious selection of blade profiles until a reasonable compromise of the flow conditions was achieved. The passage throat and blade portion downstream of it were assumed to control the exit flow angle. For the leading-edge sections, high-speed NACA series 65 airfoil nose sections were used. In the channel portion of the blade the surface velocities were calculated using the stream-filament technique of reference 5. In the channel portion of the blades the maximum suction-surface Mach number and ratio of maximum suction-surface velocity to exit velocity were 1.08 and 1.37, respectively.

The design blade profiles obtained in this manner and those of the downstream stator are shown in figure 5.

Downstream-Stator Design

The variation in hub Mach number and flow angle at the entrance to the downstream stator between engine take-off and cruise conditions is reported in reference 3. From take-off to cruise the hub entrance Mach number increased from 0.44 to 0.63 and the hub entrance flow angle measured from the axial direction increased from 26° to 32° . Reference 6 indicates that an NACA series 65-(12)10 airfoil with a maximum meanline height 0.05515 of the chord would efficiently turn the flow to axial over this range of entrance Mach number and flow angle. This airfoil section was, therefore, used for the downstream stator. The variation in stagger of the airfoil with radius was determined by the variation in entrance flow angle with radius shown in figure 4. The design angle of incidence varied from -0.6° at the hub to -3.4° at the tip.

Blade Solidity and Aspect Ratio

References 7 and 8 were used as a guide in selecting the blade solidities of the first two stators and the rotors. The solidity of the

downstream stator was obtained from reference 6. The aspect ratios were selected to give a good mechanical design for the turbine. The resulting solidities and aspect ratios based on axial chord were as follows:

	Solidity			Mean
	Hub	Mean	Tip	aspect ratio
First stator First rotor Second stator Second rotor Downstream stator	1.36 1.68 2.00 2.09 1.57	1.24 1.50 1.71 1.59 1.14	1.14 1.35 1.50 1.25	1.940 2.487 2.729 3.150 3.431

Turbine

The turbine was designed for the following conditions:

	Turbine design conditions	Turbine equivalent design conditions
Work, Btu/lb	131	32.25
Weight flow, lb/sec	158	39.65
Rotative speed, rpm	6100	3027
Inlet temperature, OR	2160	518.7
Inlet pressure, in. Hg abs	248.3	29.92

A schematic diagram of the geometry employed in the turbine design is shown in figure 2. In the design the turbine frontal area was required to be no larger than the compressor frontal area. Because of this restriction on turbine frontal area and the low design rotative speed, the velocity diagrams were obtained by keeping the tip diameter of the turbine constant and obtaining all the area divergence through the turbine from the inner wall. The tip diameter of the turbine was constant at 33.5 inches; the annular area increased through the turbine with the inner shroud having a cone half-angle of 27.6°. The hub-tip radius ratios at the exit of the first stator and last rotor were, respectively, 0.813 and 0.613. The hub-tip radius ratio at the exit of the downstream stator was 0.539. The design work output of the turbine was split 67/33 between the first and second stages, respectively.

METHODS AND PROCEDURES

The turbine was operated with a measured inlet pressure p_0^1 of approximately 35 inches of mercury absolute and an inlet temperature T_0^1 of 700^0 R for equivalent rotative speeds of 20, 40, 60, 70, 80, 90, 100, 110, 120, and 130 percent of the design value. A range of rating pressure ratios $p_0^1/p_{6,x}^1$ from 1.4 to 5.6 was investigated.

The method used to convert turbine test conditions to equivalent operating conditions based on NACA standard sea-level conditions is given in reference 9. The equivalent work output and brake internal efficiency for the over-all performance are based on measured torque values.

The over-all turbine performance rating (efficiency $\eta_{0-6,x}$, see appendix) was based on the calculated exit pressure $p_{6,x}^{\prime}$, defined as the static pressure behind the downstream stator plus the velocity pressure corresponding to the axial component of the absolute velocity. This calculated value of turbine-exit pressure charges the turbine for the energy of the tangential component of exit velocity. This pressure is calculated from the energy equation and continuity by using the known annulus area at the measuring station and measured values of weight flow, static pressure, total (stagnation) pressure, and total temperature. The derivation of the equation to calculate p_x^{\prime} is given in the appendix.

The total-temperature and pressure readings at stations 0, 5, and 6 were arithmetically averaged for a single reading of temperature and pressure at these stations. In presenting the static-pressure distribution through the turbine, the arithmetic average of the hub-wall static-pressure readings were used for stations 1 to 6. In calculating $p_{5,x}^{i}$ and $p_{6,x}^{i}$, the wall static-pressure readings at both the hub and tip were arithmetically averaged for a single reading.

The indicated temperature readings obtained from the spike-type thermocouple probes were corrected for Mach number effects. The indicated pressure readings obtained from the shielded total-pressure probes were corrected for both Mach number and Reynolds number effects.

In addition to the efficiency used to rate the turbine, three other turbine efficiencies are defined in the appendix. These efficiencies are useful in evaluating the downstream-stator performance in terms of its effect on over-all turbine performance. The difference between the efficiencies η_{0-5} and η_{0-6} measures the effect on the turbine performance of the total-pressure loss across the downstream stator. The difference between the efficiencies η_{0-5} and $\eta_{0-5,x}$ is a measure of

the amount of energy of the tangential component of velocity leaving the last rotor (entering the downstream stator) and shows the effect of this energy on turbine performance. Similarly, the difference between the efficiencies η_{0-6} and $\eta_{0-6,x}$ is a measure of the energy of the tangential component of velocity leaving the downstream stator and its effect on turbine performance. The difference between efficiencies η_{0-5} and $\eta_{0-6,x}$ is a measure of the total effectiveness of the downstream stator.

The effect on turbine performance of the downstream stator can be determined from the turbine efficiency ratings defined in the appendix and discussed previously. Indirectly, the downstream-stator performance can be determined from the difference of these efficiencies, but a more direct measure of its performance would be desirable. Accordingly, a recovery rating is defined in the appendix as follows:

Recovery factor =
$$\ln \frac{p_6^i, x}{p_5^i, x} / \ln \frac{p_5^i}{p_5^i, x}$$
 (14)

This recovery factor is the ratio of the reduction in entropy achieved by using the downstream stator to the entropy increase that would have occurred if all the energy of the tangential velocity at the exit of the last rotor had been lost. Since an entropy increase represents a loss, this ratio represents the effectiveness of the downstream stator in recovering the energy of the tangential velocity at the exit of the last rotor or the effectiveness of the stator in preventing this energy from representing a loss. This recovery factor can never exceed unity (complete recovery) but may have a negative value if the total-pressure loss across the downstream stator becomes great enough.

RESULTS AND DISCUSSION

Over-All Performance

The over-all performance of the turbine is presented in figure 6 as a plot of equivalent work against the flow parameter (wN/608) ϵ for constant values of equivalent speed N/ $\sqrt{\theta_{\rm CT}}$ and rating pressure ratio $p_0'/p_{6,x}'$. In addition, contours of constant brake internal efficiency $\eta_{0-6,x}$ are shown.

At equivalent design work and speed, an efficiency of 0.81 was obtained at a rating pressure ratio of approximately 3.8. A maximum efficiency of 0.85 occurred at 130 percent of equivalent design speed and a work output of 36.5 Btu per pound, corresponding to a rating pressure ratio of approximately 4.4.

The variation of equivalent weight flow with rating pressure ratio for the equivalent speeds investigated is shown in figure 7. The value for equivalent design weight flow is indicated on the weight-flow ordinate. At equivalent design speed and the rating pressure ratio (3.8) corresponding to equivalent design work, the turbine weight flow was 98 percent of the equivalent design weight flow. Choking weight flow, indicated when the curves have zero slope, was obtained above a rating pressure ratio of 3.4 for all speeds. The magnitude of the choking weight flow was the same for all speeds. This indicates that the first stator choked prior to any other blade row over the range of speeds investigated and controlled the weight flow passed by the turbine.

The variation of equivalent torque with rating pressure ratio for the equivalent speeds investigated is shown in figure 8. At the higher speeds and pressure ratios the slope of these curves is zero. This could result from either turbine limiting loading or choking in the downstream stator or both. Limiting loading (ref. 10) occurs when an increase in pressure ratio across a blade row does not produce an increase in the tangential loading or force. In a multistage turbine, limiting loading for the entire turbine occurs after the last rotor has choked and when a decrease in pressure at the exit of this blade row does not produce an increase in the torque output. The choking characteristics of the turbine at 90, 100, and 130 percent of equivalent design speed will be discussed subsequently in detail and integrated with the limiting-loading question. These speeds were considered because they cover the range of speeds over which the torque curves obtained a zero slope.

Choking Characteristics

Choking in a blade row, or downstream of the blade row, is indicated when the static pressure ahead of the blade row remains constant with increasing rating pressure ratio p'/p',x. Choking in a given blade row rather than some point downstream of the blade row occurs if the static pressure ahead of the blade row becomes constant while those downstream continue to fall. The static-pressure distributions at the hub of the blades against rating pressure ratio poppia,x for 90, 100, and 130 percent of equivalent design speed are shown in figures 9(a), (b), and (c), respectively. The static pressure at each station has been divided by the inlet total pressure in order to eliminate the effect of the small fluctuations in inlet total pressure encountered while testing the turbine. The data shown in figure 9 indicates for all three speeds that, excepting the downstream stator, the blade rows choke successively starting with the first stator as the rating pressure ratio increases. The change in slope from negative to zero at station 1, indicating the first stator chokes, is not very pronounced. The decrease

in flow area between the entrance of the first stator and its throat is large. Consequently, the Mach number and static-pressure variation at the entrance to the stator is small, making this static-pressure variation a poor criterion of choking in this blade row. However, the weight-flow curves of figure 7 show, as mentioned previously, that the first stator definitely chokes first at these speeds.

At 90 percent of equivalent design speed (fig. 9(a)) the static pressures at station 5, ahead of the downstream stator, decreased over the whole range of rating pressure ratio $p_0'/p_{6,x}'$. The downstream stator, therefore, does not choke at this speed. Since the downstream stator did not choke, the torque curve for this speed in figure 8 obtained a zero slope because the turbine reached limiting loading. The same conditions prevailed at 100 and 130 percent of equivalent design speed (figs. 9(b) and (c), respectively).

Downstream-Stator Performance

The effect of the downstream-stator performance on the over-all turbine performance is shown in figure 10, where the efficiencies defined in the appendix are shown against the equivalent shaft work for speeds from 70 to 130 percent of equivalent design speed. The efficiency η_{0-5} rates the turbine on the basis of the measured total pressure ahead of the stator, which includes the total velocity head. Efficiency $\eta_{0-5,x}$ shows the effect on turbine performance of charging the turbine with the energy of the tangential velocity ahead of the stator. Efficiency η_{0-6} shows the effect of the total-pressure loss across the stator, while efficiency $\eta_{0-6,x}$ shows the additional effect of charging the turbine with the energy of the tangential velocity at the exit of the stator. The difference between efficiency η_{0-5} and the efficiency used to rate the turbine $\eta_{0-6,x}$ shows the total effect of the stator on turbine performance.

At equivalent design work and speed (fig. 10(d)), the stator recovery was good. The drop in turbine efficiency due to total-pressure loss across the stator amounted to 0.006, and the stator-exit tangential-velocity energy represented another drop of 0.005. The total drop in turbine efficiencies, 0.011, is small in comparison with the potential drop, 0.048, that would result if none of the kinetic energy of the second rotor-exit tangential velocity were recovered.

The shaded area between efficiencies η_{0-6} and $\eta_{0-6,x}$, showing the drop in turbine efficiency due to the tangential velocity of the gas leaving the stator, was small over the range of conditions shown. This indicates that the stator left very little tangential-velocity energy in the gas at any of these operating conditions.

The total drop in turbine efficiency from η_{0-5} to $\eta_{0-6,x}$ was small over a broad range of work output at low speeds. However, as the speed increased, the range of work output over which the stator performed well was limited and moved to higher work outputs. The poor stator performance at the higher speeds and low work outputs was probably the result of large negative angles of attack on the stator. At high work output, the poor stator performance probably resulted from high inlet Mach numbers. In both instances, the large drop in turbine efficiency resulted from total-pressure loss across the stator and not as a result of large tangential components of velocity at the stator exit.

A recovery factor for the stator which measures the effectiveness of the downstream stator in recovering the tangential-velocity energy entering the stator is defined in the appendix. This recovery factor against the equivalent shaft work for speeds from 70 to 130 percent of equivalent design speed is shown in figure 11. This recovery factor can never exceed unity (full recovery) but does have a negative value when the total-pressure loss across the stator becomes great enough.

At equivalent design work and speed (fig. ll(d)), the stator recovery was 0.78, which for practical purposes is the amount of entrance tangential-velocity energy recovered.

The stator recovery patterns follow the effects noted in figure 10 of stator performance on turbine efficiency. From figure 11 it is seen that good recovery over a broad range of work output was obtained at low speed, with the range of work output over which the stator has good recovery decreasing and moving to higher work outputs as the speed increases.

CONCLUDING REMARKS

The over-all turbine efficiency $\eta_{0-6,x}$ at equivalent design work and speed was well below the value anticipated in the design of the turbine. The low efficiency obtained does not necessarily preclude the possibility that good turbine efficiency could be obtained with some other turbine design. Perhaps higher turbine efficiency could be obtained if a turbine were designed accounting for the three dimensionality of the flow, as in reference 11, and with closer control of the blade loading, as in reference 12. It does appear, however, that the blade design procedure used for the turbine herein was inadequate for a turbine with such critical aerodynamic limits.

The downstream-stator performance was, in general, very good.

Near-axial discharge was obtained over a wide operating range; and, when

properly matched to the rotor-discharge Mach number and flow angle, excellent recovery of the energy of the tangential velocity leaving the last rotor was obtained.

SUMMARY OF RESULTS

From an experimental investigation of a high-work-output, low-blade-speed, two-stage turbine with a downstream stator, operated over a range of equivalent speed and total-pressure ratio at inlet conditions of 35 inches of mercury absolute and 700° R, the following results were obtained:

- 1. At equivalent design speed and work, the turbine passed 0.98 of the equivalent design weight flow. The brake internal efficiency at this point was 0.81 and occurred at a rating pressure ratio of 3.8.
- 2. A maximum efficiency of 0.85 occurred at 130 percent of equivalent design speed and a work output of 36.5 Btu per pound, corresponding to a rating pressure ratio of approximately 4.4.
- 3. At 90 percent of equivalent design speed and above, the blade rows, with the exception of the downstream stator, choked successively starting with the first stator as the over-all pressure ratio was increased.
- 4. Turbine limiting loading was observed for speeds from 90 to 130 percent of equivalent design speed.
- 5. The downstream stator left very little energy in the form of tangential velocity in the gas at any operating condition.
- 6. Recovery of the energy of the tangential velocity at the entrance to the downstream stator was good over a broad range of work output near 70 percent of equivalent design speed. With increasing rotative speed, the best recovery was reached over a very limited range of work output. In general, the best recovery for the stator moved to a higher work output with an increase in rotative speed.
- 7. At equivalent design work and speed, the downstream stator recovered 0.78 of the energy of the tangential velocity entering the stator. The energy of this tangential velocity amounted to 4.8 points in turbine efficiency.

Lewis Flight Propulsion Laboratory
National Advisory Committee for Aeronautics
Cleveland, Ohio, August 17, 1955

APPENDIX - DERIVATION OF TOTAL-PRESSURE, EFFICIENCY, AND

DOWNSTREAM-STATOR RECOVERY EQUATIONS

Total Pressure

The one-dimensional equation for calculating the total pressure p_{x}^{\prime} based on the axial component of velocity at the exit of a blade row can be derived form a combination of the following equations:

Energy:
$$T_{x}' = T + \frac{v_{x}^{2}}{2gJc_{p}}$$
 (1)

Continuity:
$$W = \rho V_X A$$
 (2)

State:
$$p = \rho RT$$
 (3)

Isentropic relations:
$$\frac{T}{T'} = \left(\frac{p}{p'}\right)^{\frac{\gamma-1}{\gamma}}$$
 (4)

and

$$\frac{T_{X}^{i}}{T^{i}} = \left(\frac{p_{X}^{i}}{p^{i}}\right)^{\Upsilon} \tag{5}$$

Based on equations (1) to (5), the following equation for the axial total pressure can be obtained:

$$p_{x}' = p \left[1 + \frac{(\gamma - 1)}{2\gamma g} \left(\frac{w}{A} \right)^{2} \frac{RT'}{p^{2}} \left(\frac{p}{p'} \right)^{\gamma} \right]^{\frac{\gamma}{\gamma - 1}}$$
(6)

The total pressure p_X^{\prime} at the exit of a blade row can be calculated from equation (6) from the known values of w, A, p, p', and T'. The kinetic energy contained in the exit tangential-velocity component is considered a loss when the turbine efficiency is based on the exit total pressure p_X^{\prime} .

Efficiency Ratings

For the purpose of evaluating the performance of the turbine and downstream stator, four different efficiencies were calculated. The expansion process upon which the four definitions of efficiency are based is depicted in the temperature-entropy diagram of figure 12. The four efficiencies calculated for the turbine are as follows:

$$\eta_{O-5} = \frac{c_{p}(T_{O}^{i} - T_{5}^{i})}{c_{p}[T_{O}^{i} - (T_{5}^{i})_{I}]} = \frac{E}{c_{p}T_{O}^{i}\left[1 - \left(\frac{p_{5}^{i}}{p_{O}^{i}}\right)^{\gamma}\right]}$$
(7)

$$\eta_{0-5,x} = \frac{c_{p}(T_{0}^{7} - T_{5}^{7})}{c_{p}[T_{0}^{7} - (T_{5}^{7})_{II}]} = \frac{E}{c_{p}T_{0}^{7}\left[1 - \left(\frac{p_{5,x}^{7}}{p_{0}^{7}}\right)^{7}\right]}$$
(8)

$$\eta_{O-6} = \frac{c_{p}(T_{O}^{i} - T_{6}^{i})}{c_{p}[T_{O}^{i} - (T_{6}^{i})_{I}]} = \frac{E}{c_{p}T_{O}^{i}\left[1 - \left(\frac{p_{6}^{i}}{p_{O}^{i}}\right)^{\gamma}\right]}$$
(9)

$$\eta_{O-6,x} = \frac{c_{p}(T_{O}^{i} - T_{6}^{i})}{c_{p}[T_{O}^{i} - (T_{6}^{i})_{II}]} = \frac{E}{c_{p}T_{O}^{i}\left[1 - \left(\frac{p_{6,x}^{i}}{p_{O}^{i}}\right)^{\gamma}\right]}$$
(10)

where $c_p(T_0'-T_5')$ and $c_p(T_0'-T_6')$ are calculated from the weight-flow, rotative-speed, and torque measurements.

Downstream-Stator Recovery Factor

The downstream-stator recovery factor was determined in the following manner: An entropy increase $\Delta S_{5-5,x}$ (fig. 12) would occur if none

16 NACA RM E55H16

of the energy of the tangential velocity at the exit of the second rotor $V_{5,u}^2/2gJ$ were recovered. If a downstream stator were employed, the entropy increase would be $\Delta S_{5-6,x}$. (The stator is charged with the entropy increase due to the energy of the tangential velocity at the exit of the stator $V_{6,u}^2/2gJ$.) The difference between the entropy increases $\Delta S_{5-5,x} - \Delta S_{5-6,x}$ represents the reductions in entropy gained by using the stator. The ratio then of this entropy decrease $\Delta S_{5-5,x} - \Delta S_{5-6,x}$ to the entropy increase $\Delta S_{5-5,x}$ that would have occurred if all the energy of $V_{5,u}^2/2gJ$ had been lost is a measure of the total effectiveness of the stator in preventing the energy $V_{5,u}^2/2gJ$ from representing a loss. For all practical purposes the ratio also represents the amount of this energy recovered by the stator. The ratio then that was used to represent the effectiveness of the stator is:

Recovery factor =
$$\frac{\Delta S_{5-5,x} - \Delta S_{5-6,x}}{\Delta S_{5-5,x}}$$
 (11)

This ratio, representing the effectiveness of the stator, can never exceed unity (complete recovery) but may have a negative value if the total-pressure loss across the stator becomes great enough.

The recovery factor was calculated from the measured p' and calculated p_X' at stations 5 and 6. The derivation of the equation used for this purpose is as follows: With the total temperature constant, the entropy increases can be written:

$$\Delta S_{5-5,x} = \frac{R}{J} \ln \frac{p_5'}{p_{5,x}'}$$
 (12)

and

$$\Delta S_{5-6,x} = \frac{R}{J} \ln \frac{p_5'}{p_{6,x}'}$$
 (13)

If equations (12) and (13) are substituted into the recovery factor, equation (11) presents the recovery factor in terms of the measured total pressures p' and calculated total pressures p'_{x} . Thus,

Recovery factor =
$$\ln \frac{p_6^!, x}{p_5^!, x} / \ln \frac{p_5^!}{p_5^!, x}$$
 (14)

REFERENCES

- 1. English, Robert E., Silvern, David H., and Davison, Elmer H.: Investigation of Turbines Suitable for Use in a Turbojet Engine with High Compressor Pressure Ratio and Low Compressor-Tip Speed. I-Turbine-Design Requirements for Several Engine Operating Conditions. NACA RM E52Al6, 1952.
- 2. Davison, Elmer H., and English, Robert E.: Investigation of Turbines Suitable for Use in a Turbojet Engine with High Compressor Pressure Ratio and Low Compressor-Tip Speed. II Velocity-Diagram Study of Turbine for Engine Operation with Constant Exhaust-Nozzle Area. NACA RM E52D14, 1952.
- 3. English, Robert E., and Davison, Elmer H.: Investigation of Turbines Suitable for Use in a Turbojet Engine with High Compressor Pressure Ratio and Low Compressor-Tip Speed. III Velocity-Diagram Study of Two-Stage and Downstream-Stator Turbines for Engine Operation at Constant Rotative Speed. NACA RM E52G15, 1952.
- 4. Davison, Elmer H., and English, Robert E.: Investigation of Turbines Suitable for Use in a Turbojet Engine with High Compressor Pressure Ratio and Low Compressor-Tip Speed. IV Effect of Increasing Blade Speed on Velocity Diagrams of Turbine for Engine Operation at Constant Rotative Speed. NACA RM E52H13, 1952.
- 5. Huppert, M. C., and MacGregor, Charles: Comparison Between Predicted and Observed Performance of Gas-Turbine Stator Blade Designed for Free-Vortex Flow. NACA TN 1810, 1949.
- 6. Herrig, L. Joseph, Emery, James C., and Erwin, John R.: Systematic Two-Dimensional Cascade Tests of NACA 65-Series Compressor Blades at Low Speeds. NACA RM L51G31, 1951.
- 7. Zweifel, O.: Optimum Blade Pitch for Turbo-Machines with Special Reference to Blades of Great Curvature. The Eng. Digest, vol. 7, no. 11, Nov. 1946, pp. 358-360; cont., vol. 7, no. 12, Dec. 1946, pp. 381-383.
- 8. Heller, Jack A., Whitney, Rose L., and Cavicchi, Richard H.: Experimental Investigation of a Conservatively Designed Turbine at Four Rotor-Blade Solidities. NACA RM E52C17, 1952.
- 9. Rebeske, John J., Jr., Berkey, William E., and Forrette, Robert E.:
 Over-All Performance of J35-A-23 Two-Stage Turbine. NACA RM
 E51E22, 1951.

- 10. Hauser, Cavour H., and Plohr, Henry W.: Two-Dimensional Cascade Investigation of the Maximum Exit Tangential Velocity Component and Other Flow Conditions at the Exit of Several Turbine-Blade Designs at Supercritical Pressure Ratios. NACA RM E51F12, 1951.
- ll. Stewart, Warner L.: Analytical Investigation of Flow Through High-Speed Mixed-Flow Turbine. NACA RM E51H06, 1951.
- 12. Whitney, Warren J., Monroe, Daniel E., and Wong, Robert Y.: Investigation of Transonic Turbine Designed for Zero Diffusion of Suction-Surface Velocity. NACA RM E54F23, 1954.

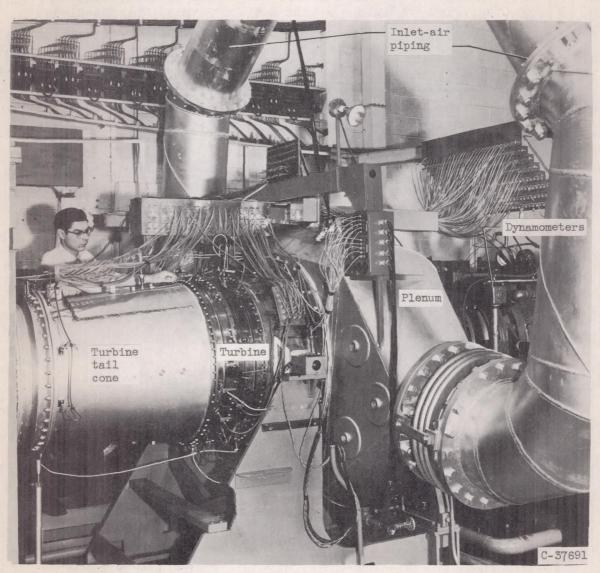


Figure 1. - Installation of turbine in full-scale turbine component test facility.

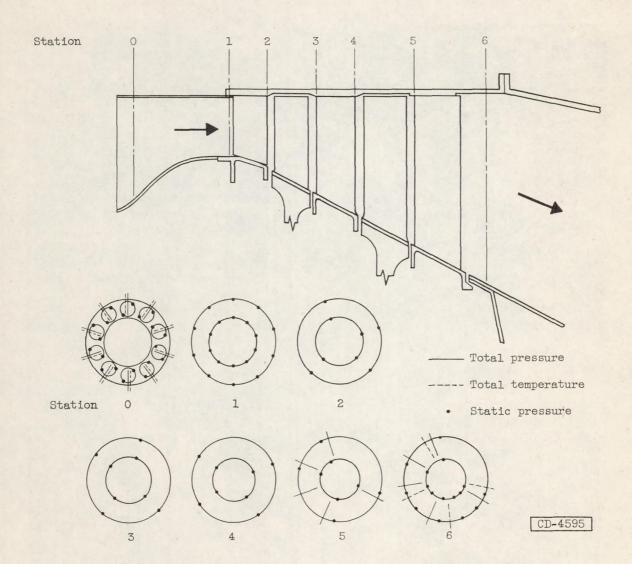
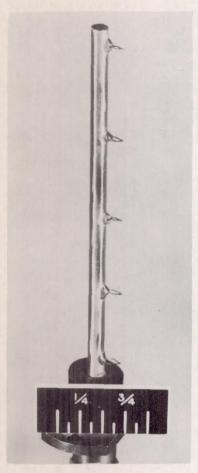
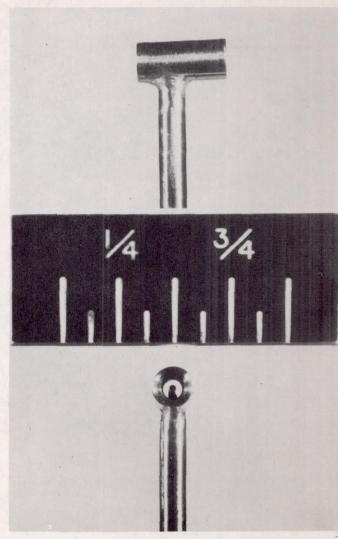


Figure 2. - Schematic diagram of turbine showing instrumentation.



(a) Total-temperature rake.

C-39557



(b) Total-pressure probe.

Figure 3. - Typical total-temperature rake and total-pressure probe.

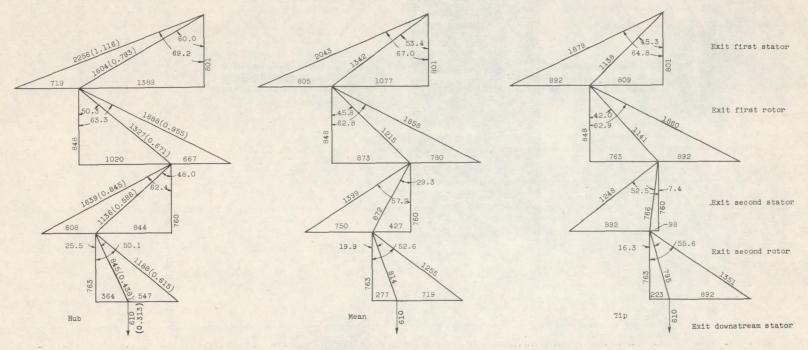


Figure 4. - Design velocity diagrams. Numbers in parentheses are Mach numbers based on local velocity of sound; velocities are in feet per second; angles are in degrees.

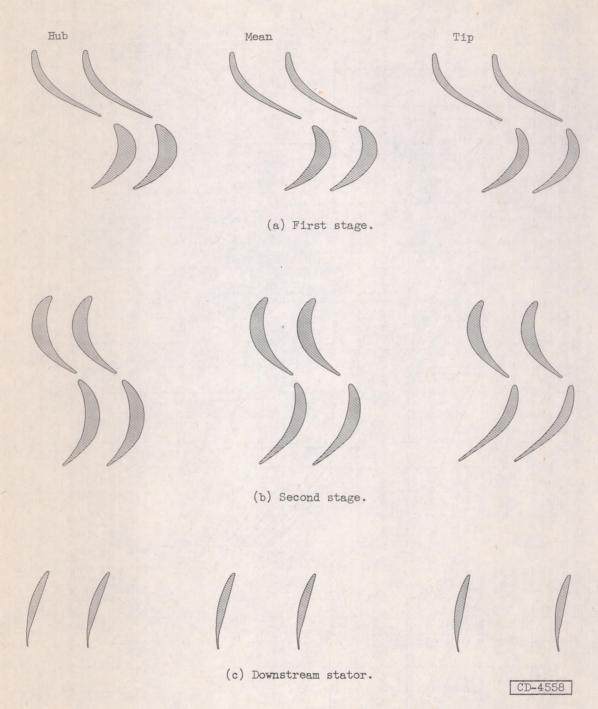


Figure 5. - Design blade and channel shapes for two-stage turbine with downstream stator.

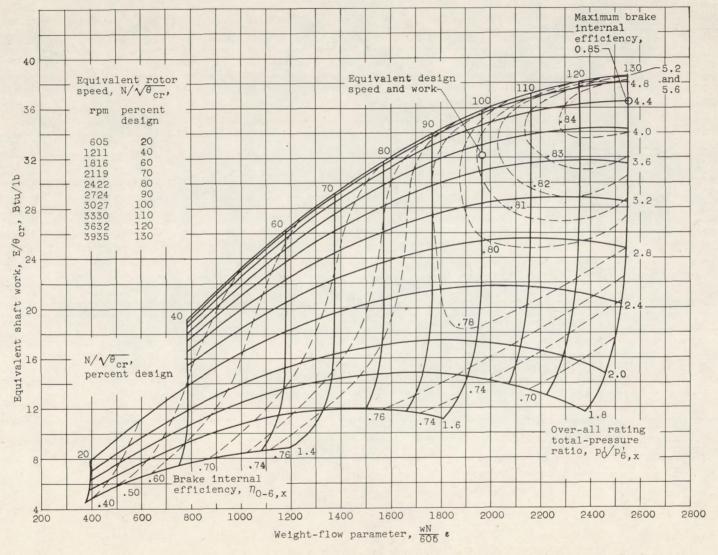


Figure 6. - Over-all performance of turbine. Turbine-inlet pressure, 35 inches of mercury absolute; turbine-inlet temperature, 700° R.



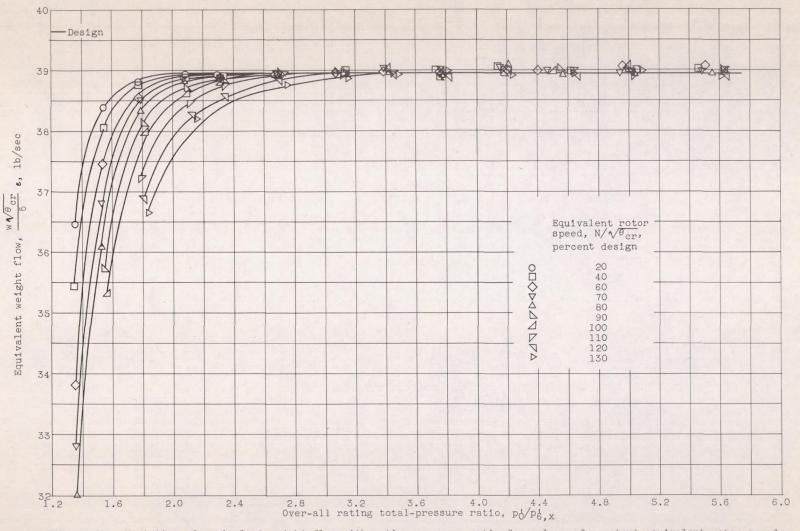


Figure 7. - Variation of equivalent weight flow with rating pressure ratio for values of constant equivalent rotor speed.

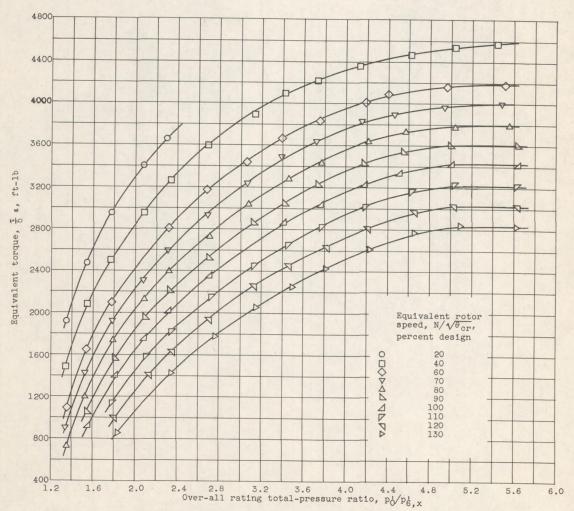


Figure 8. - Variation of equivalent torque with rating pressure ratio for values of constant equivalent rotor speed.

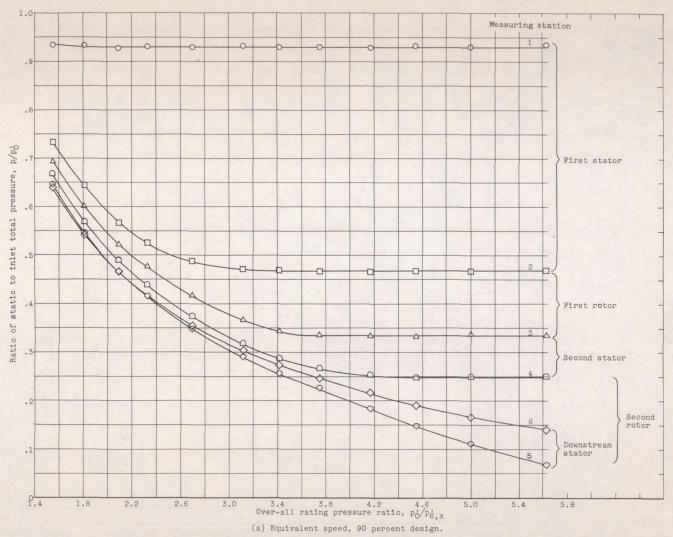


Figure 9. - Variation of hub static pressure with rating pressure ratio at several measuring stations.

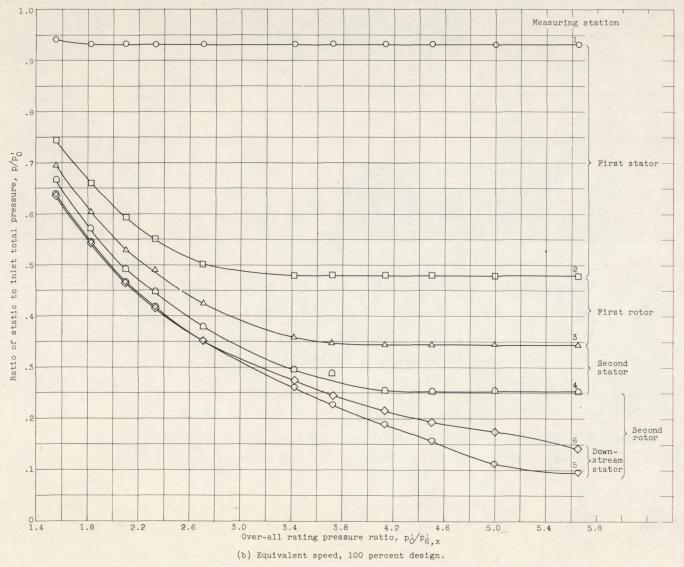


Figure 9. - Continued. Variation of hub static pressure with rating pressure ratio at several measuring stations.

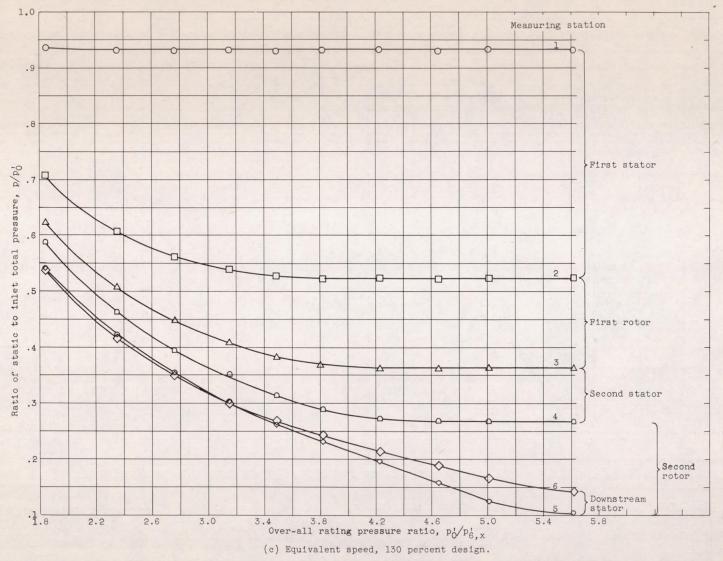
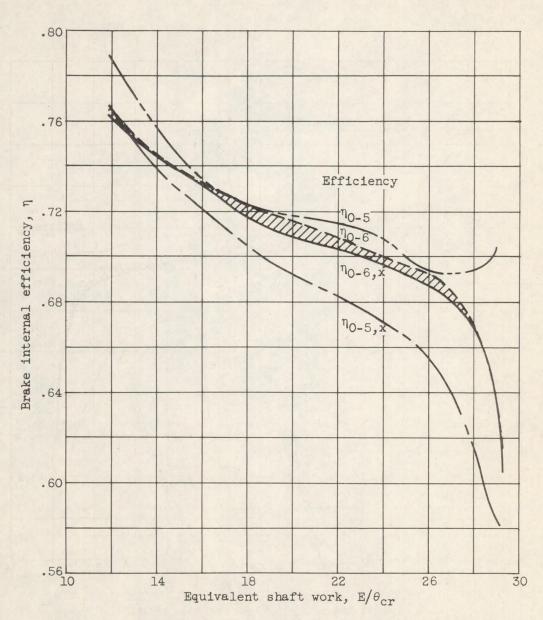
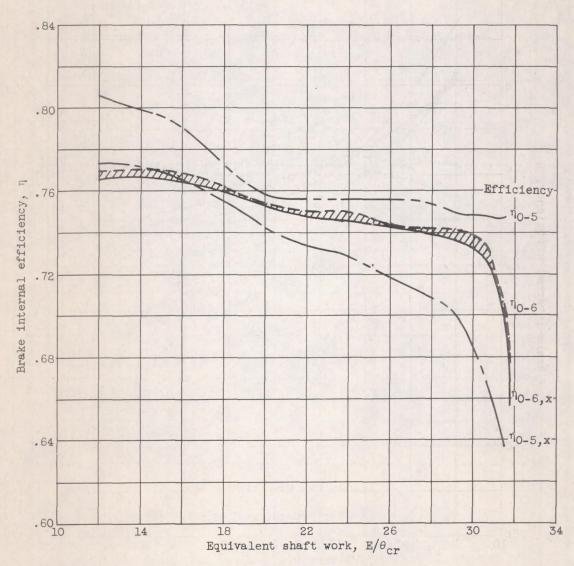


Figure 9. - Concluded. Variation of hub static pressure with rating pressure ratio at several measuring stations.



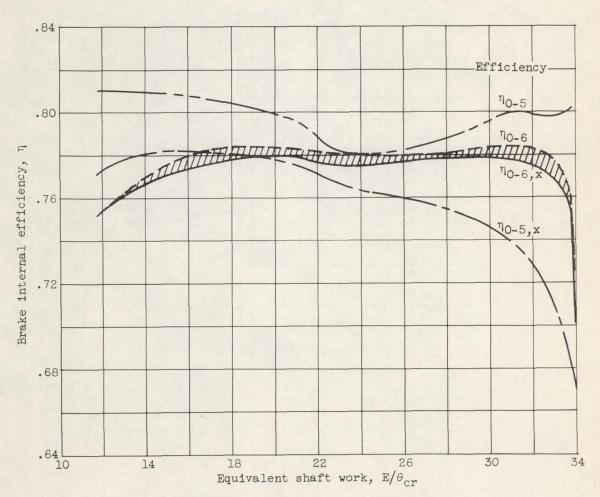
(a) Equivalent speed, 70 percent design.

Figure 10. - Effect of turbine speed and work output on downstream-stator performance.



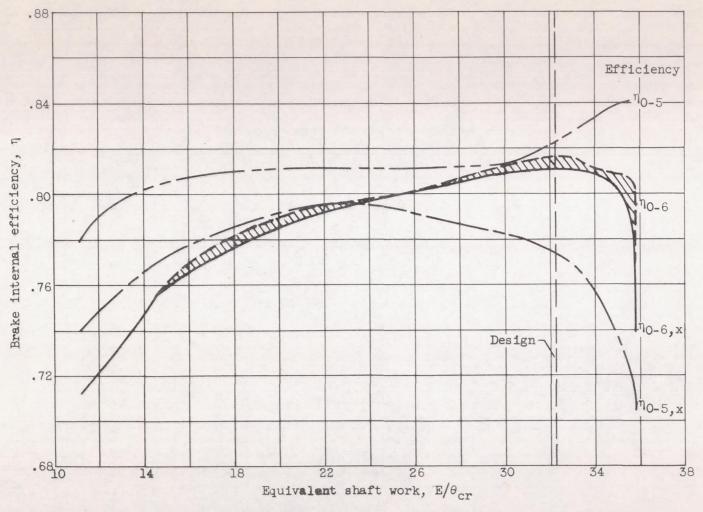
(b) Equivalent speed, 80 percent design.

Figure 10. - Continued. Effect of turbine speed and work output on downstream-stator performance.



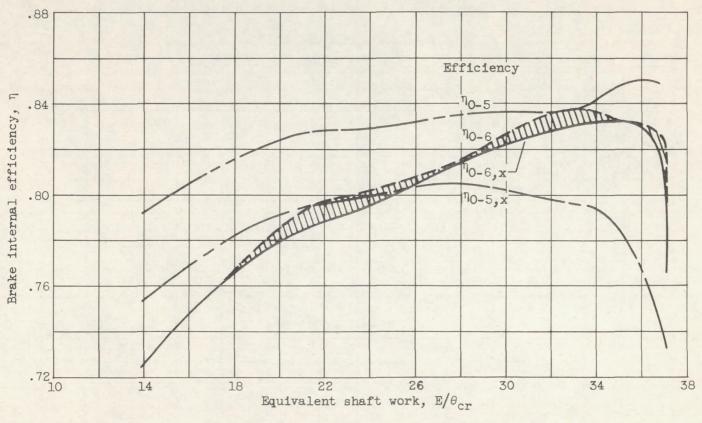
(c) Equivalent speed, 90 percent design.

Figure 10. - Continued. Effect of turbine speed and work output on downstream-stator performance.



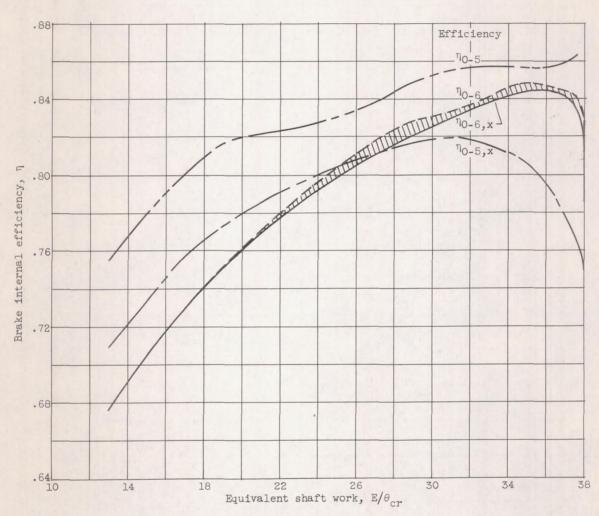
(d) Equivalent speed, 100 percent design.

Figure 10. - Continued. Effect of turbine speed and work output on downstream-stator performance.



(e) Equivalent speed, 110 percent design.

Figure 10. - Continued. Effect of turbine speed and work output on downstream-stator performance.



(f) Equivalent speed, 120 percent design.

Figure 10. - Continued. Effect of turbine speed and work output on downstream-stator performance.

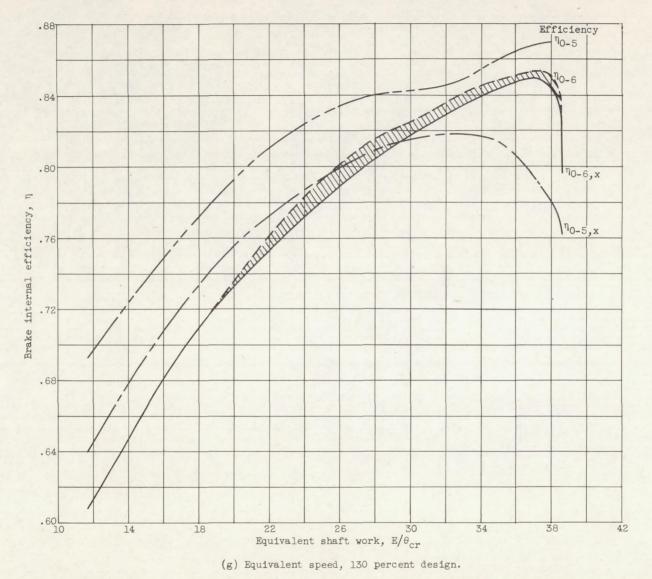
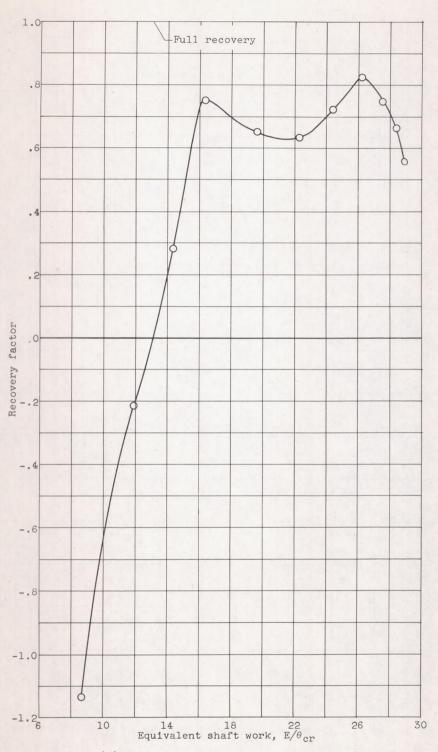
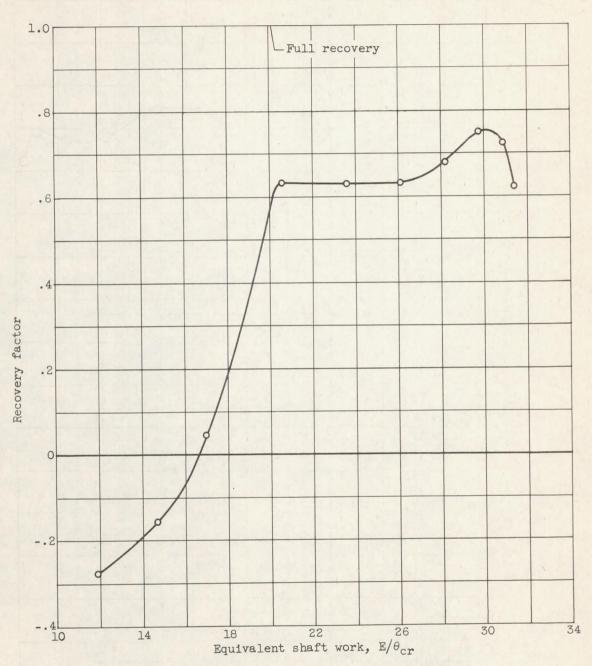


Figure 10. - Concluded. Effect of turbine speed and work output on downstream-stator performance.



(a) Equivalent speed, 70 percent design.

Figure 11. - Downstream-stator recovery of tangential-velocity energy.

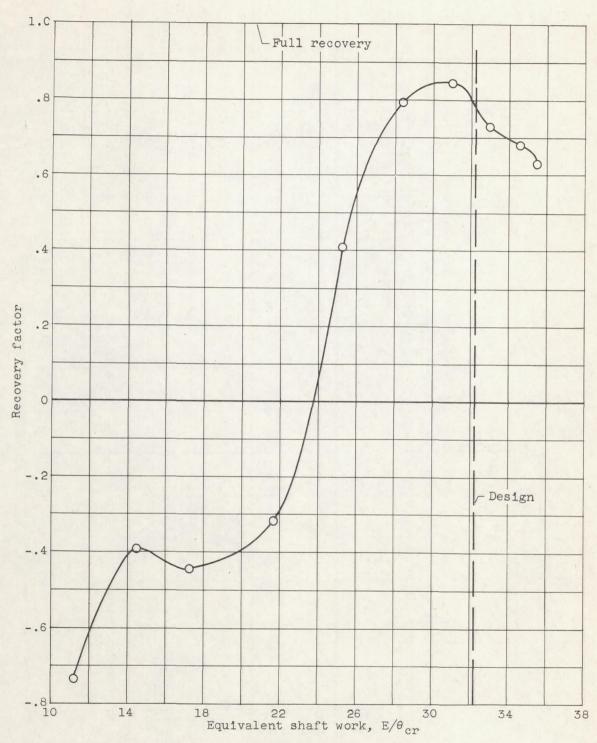


(b) Equivalent speed, 80 percent design.

Figure 11. - Continued. Downstream-stator recovery of tangential-velocity energy.

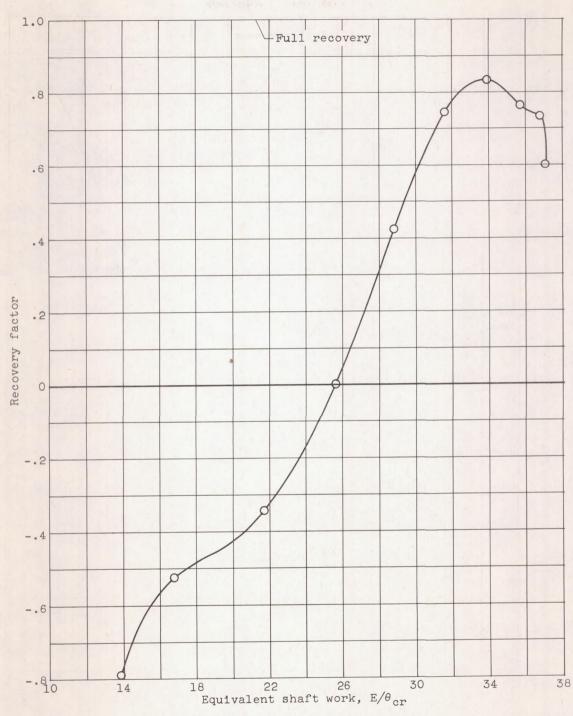
(c) Equivalent speed, 90 percent design.

Figure 11. - Continued. Downstream-stator recovery of tangential-velocity energy.



(d) Equivalent speed, 100 percent design.

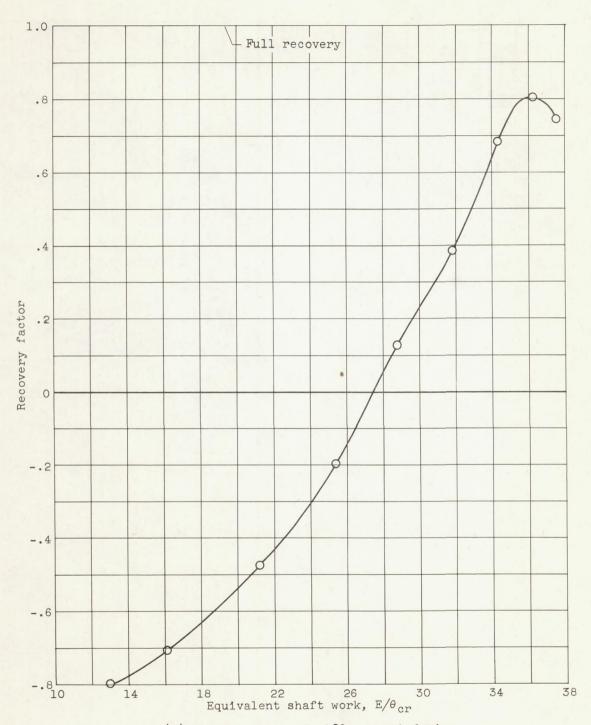
Figure 11. - Continued. Downstream-stator recovery of tangential-velocity energy.



(e) Equivalent speed, 110 percent design.

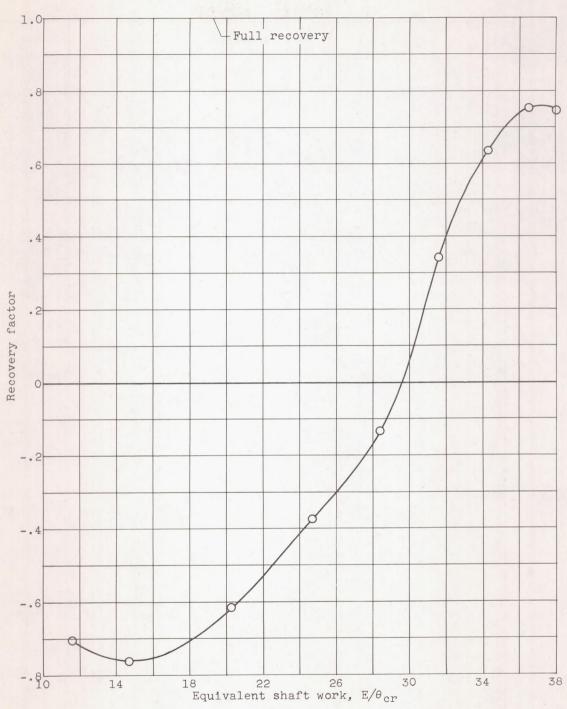
Figure 11. - Continued. Downstream-stator recovery of tangential-velocity energy.

NACA RM E55H16



(f) Equivalent speed, 120 percent design

Figure 11. - Continued. Downstream-stator recovery of tangential-velocity energy.



(g) Equivalent speed, 130 percent design.

Figure 11. - Concluded. Downstream-stator recovery of tangential-velocity energy.

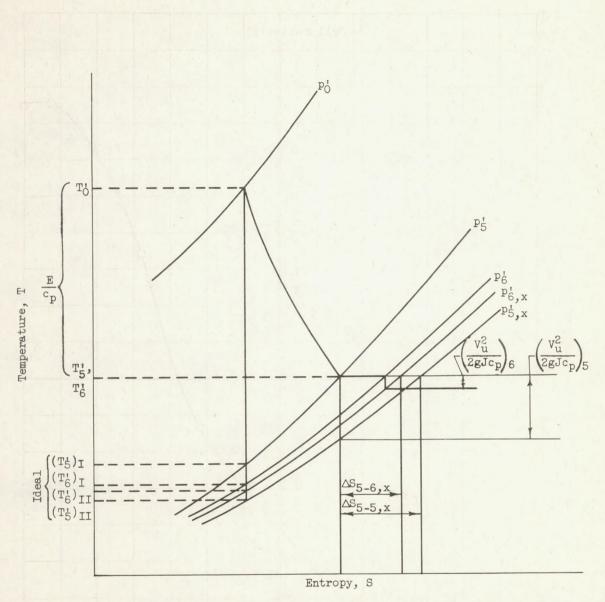


Figure 12. - Temperature-entropy diagram used to define efficiency ratings and downstream-stator recovery rating.